Powder retection with T-ray imaging

Bradley Ferguson[a,b,c], Shaohong Wang[a], Hua Zhong[a],
Derek Abbott[c] and X.-C. Zhang[a]

[a]Center for Terahertz Research,
Rensselaer Polytechnic Institute, Troy, NY 12180, USA

[b]CRC for Sensor, Signal and Information Processing,
Technology Park, Mawson Lakes Boulevard, Mawson Lakes, SA 5095, Australia

[c]Centre for Biomedical Engineering and
Department of Electrical & Electronic Engineering,
Adelaide University, SA 5005, Australia

ABSTRACT

Pulsed THz imaging systems have a number of potential advantages in inspection applications. They provide amplitude and phase information across a broad spectral range in the far-infrared, and many common packaging materials are relatively transparent in this frequency range. We use T-ray imaging to allow the identification of different powdered materials concealed inside envelopes. Using the terahertz spectral information we show that different powders may be uniquely identified.

Different thicknesses of the powders are imaged to investigate the influence of scattering on the measured THz pulses and the classification model is extended to allow it to identify different materials independent of the material thickness.

Keywords: terahertz, T-ray imaging, chirped pulse, linear-filter modelling, classification

1. INTRODUCTION

Pulsed terahertz imaging is a relatively new addition to the wide array of available imaging modalities.[1] It utilizes the terahertz, or far-infrared, region of the electromagnetic spectrum and is based upon the increasingly popular technique of terahertz time-domain spectroscopy (THz-TDS). The unique properties of THz radiation allow terahertz imaging to fill niches that are unreachable using other techniques. THz spectroscopy systems are seeing application in semi-conductor characterization,[2] gas sensing[3] and molecular probing.[4] Terahertz imaging has been demonstrated for imaging flames,[5] leaf moisture content,[6] skin burn severity,[5] tooth cavities[7] and skin cancer.[8]

The detection of potentially hazardous materials inside mail and luggage has become a top worldwide priority in recent years. Bacterial spores such as *bacillus anthracis* have been of particular concern since they were used in suspected mail bioterrorism attacks leading to 5 deaths in 2001.[9] Several technologies are under development and on the market for detecting hazardous material in mail however the search continues for a real-time, highly sensitive, highly specific, yet general purpose imaging detection system.

Recent experiments on bacterial spores including the anthrax simulant *bacillus subtillus* have demonstrated several strong attenuation resonances in the THz frequency range. These resonances are attributed to the protein cladding of the spore.[10] These results promote the possibility of allowing automatic detection or retection of bacterial spores concealed within mail. However, detection of powdered materials presents additional difficulties compared to the previously published thin film studies. Most powders strongly scatter THz radiation. The scattering response may be frequency dependent, particularly if the particle size is close to the wavelength of the radiation (0.3 mm at 1 THz). Scattering causes particularly severe problems in THz-TDS where the time

Further author information: (Send correspondence to X.-C. Z.)
E-mail: zhangxc@rpi.edu, Telephone: 1 518 276 3096

Terahertz for Military and Security Applications, R. Jennifer Hwu, Dwight L. Woolard,
Editors, Proceedings of SPIE Vol. 5070 (2003) © 2003 SPIE · 0277-786X/03/$15.00

domain THz signal is measured and Fourier transformed to obtain the spectral response. Multiple scattering paths distort the time domain waveform and may thereby obscure resonant absorptions in the frequency domain.

For this reason, simple identification algorithms have had limited success in THz-TDS experiments and more complicated signal processing and machine learning approaches are favored. Previous work in this area for THz data analysis has been reported in determining optimal techniques for de-noising,[11,12] extracting material constants,[13,14] gas mixture analysis[15] and biological material classification.[16] Here we apply relatively simple techniques and show that we are able to classify powders concealed within envelopes despite the presence of strong scattering.

Pulsed THz imaging was used to image several powder samples to provide data for training and testing the classification system. The hardware system is described in Section 2. Section 3 describes the experiments conducted and the data obtained. The processing algorithms which were utilized to allow the identification of each powder are detailed in Section 4. Finally Section 5 presents the classification results and Section 6 presents our conclusions and avenues for future work.

2. THZ IMAGING

Pulsed terahertz imaging was first demonstrated by Hu and Nuss in 1995.[17] They used optically gated photoconductive antennas for the generation and detection of terahertz pulses. They replaced the slow scanning delay line used in THz-TDS systems with a rapid 20 Hz scanning delay line and used a digital signal processor instead of the slow lock in amplifier (LIA) to acquire and digitize the signal. The sample was then scanned in X and Y dimensions to build up an image. This system achieved an acquisition rate of 12 pixels/s with a signal to noise ratio greater than 100:1. This system was used to image leaves, bacon and semiconductor circuits.[18]

Shortly afterwards a dramatic improvement in acquisition speed was made using two-dimensional electro-optic detection of the terahertz pulse.[19] In this technique the terahertz pulse acts as a transient bias on a $\langle 110 \rangle$ oriented ZnTe crystal, inducing a polarization in the crystal. A probe laser pulse with a larger diameter than the THz beam is then modulated by the polarization-induced birefringence of the ZnTe crystal via the Pockel's effect. The two-dimensional THz field distribution is then converted to a 2D intensity modulation on the optical probe beam after it passes through a crossed polarizer (analyzer). A digital charge coupled device (CCD) camera is then used to record the optical image.

2.1. Scanning THz Imaging

Traditional T-ray imaging systems are based on THz-TDS techniques. A scanning delay line is used to offset the pump and probe beams and allow the temporal profile of the THz pulse to be measured. The sample is raster scanned in X and Y dimensions to acquire an image. These systems offer high SNR but have long acquisition times. Our system is illustrated in fig. 1.

The laser system used was a regeneratively amplified Ti:sapphire laser (Spectra Physics Hurricane) with an average output power of 700 mW, a pulse duration of 130 fs and a repetition rate of 1 kHz. The center wavelength of the laser was 802 nm and the spectral bandwidth was 4 nm. The THz emitter was a ZnTe electro-optic crystal and the THz field was generated via optical rectification of the 400 mW pump beam.

The THz beam was focused using parabolic mirrors to a spot size of 1 mm at the sample. The transmitted THz pulse was collected using parabolic mirrors and focused onto the 4 mm thick $\langle 110 \rangle$ ZnTe EO detector crystal. An optical chopper was employed to modulate the detected signal at a frequency of 182 Hz and a lock in amplifier was used to detect the signal using a time constant of 10 ms. This system achieved a dynamic range in excess of 1000.

3. EXPERIMENTAL PROCEDURE

One vital issue this work hoped to address is the ability of THz spectroscopy to detect specific powders given unknown (and variable) density, thickness and concentration. We imaged multiple thicknesses of 7 different powders. The thickness of the powders were accurately controlled using the sample holder shown in fig. 2. Approximately 10 grams of each powder were placed in a polyethylene plastic bag. Two teflon blocks were

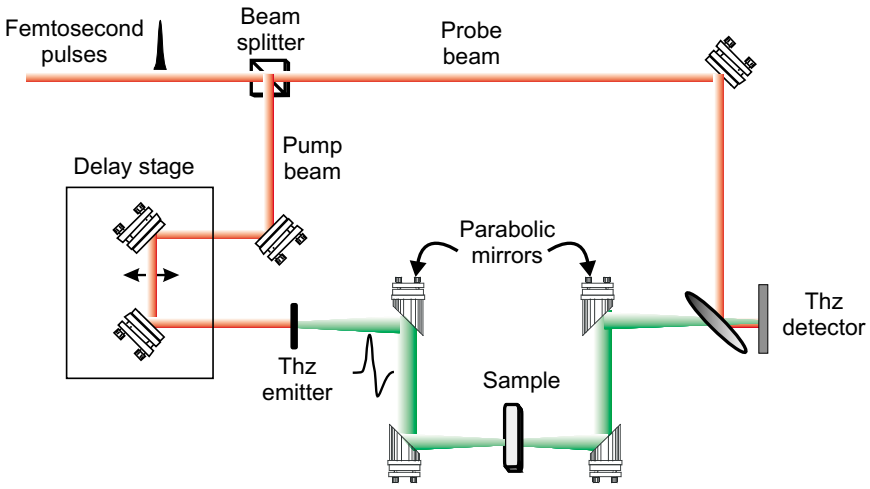

Fig. 1. Simplified hardware schematic used for scanning terahertz imaging. The sample is mounted on an X-Y translation stage to allow it to be imaged.

mounted on a manual translation stage which allowed the separation between the two blocks to be controlled. To test a given thickness of powder the teflon block spacing was set to provide the required gap (eg: 1, 2, 3, or 4 mm) and the plastic bag containing the powder was inserted between the teflon blocks. This ensured a relatively consistent powder density and reasonably accurate control of the powder thickness.

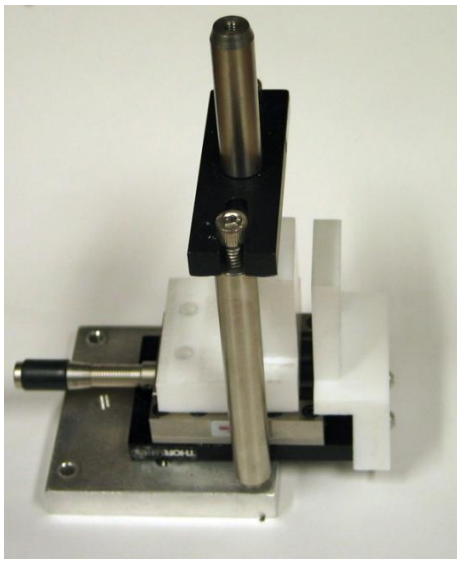

Fig. 2. Photo of the powder sample holder. One of the teflon blocks is fixed, while the position of the other is controlled using the manual translation stage. The gap between the two blocks may be adjusted to allow different thicknesses of powder to be considered.

The teflon sample holder was mounted on an X-Y translation stage and positioned in the THz beam. After a powder sample was inserted a 2D THz image of the sample was obtained. This image allowed the effects of differing scattering paths and minor variations in powder thickness and density to be observed. In general a 1D image was sufficient, and 50 pixel images (with a pixel spacing of 100 μm) could be acquired in under 30 minutes.

7 different powders were considered, these included: salt, sugar, powdered sugar, baking soda, talcum powder, flour and *bacillus thuringiensis*. Each powder was imaged at 4 different thicknesses (1, 2, 3 and 4 mm) with the exception of *bacillus thuringiensis* where the available quantity only permitted a thickness of 0.5 mm.

To test the ability of the classification system to detect powders inside envelopes a composite target was constructed. This target consisted of thin layers of 6 different powders taped onto a piece of paper to form the letters 'THz'. Each section of the characters was formed using a different powder. The target was then placed inside an envelope and imaged using the THz imaging system. A coarse step size of 5 mm was used in the x and y dimensions and the THz time domain pulse was measured at each pixel. This image took approximately 5 hours to acquire. A photo of the target is shown in fig. 3.

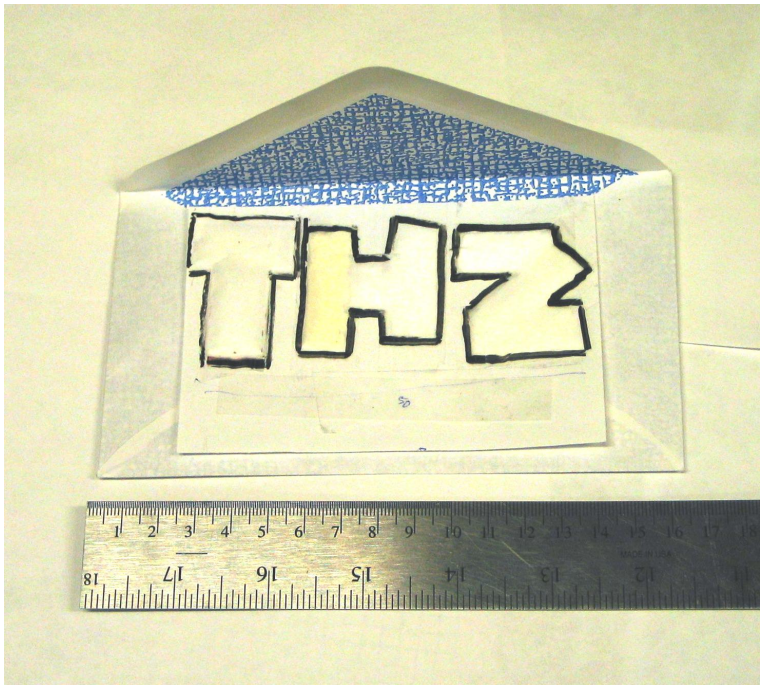

Fig. 3. Photo of the powder target. The powders were taped onto a piece of paper to form the letters 'THZ'. The letter 'T' consists of salt (upper) and sugar (lower), the letter 'H' consists of flour (left) and powdered sugar (right and center), and the letter 'Z' consists of baking soda (upper) and talcum powder (lower and center).

4. CLASSIFICATION

The ultimate goal in all terahertz systems is to extract information about the sample under test. This information may be the frequency dependent index of refraction for a semiconductor wafer or the resonant absorption frequencies for gas sensing. For inspection imaging applications we desire to detect and differentiate between different samples based on the terahertz response.

In this paper we use a simple classifier based on the *Mahalanobis distance*.[20] This is one of a class of minimum distance classifiers. It assumes that the data for each class are normally distributed, thus the samples drawn from each class will form a cluster in N dimensions, with a center given by the mean vector, μ, and shape dependent on the covariance matrix, Σ. We form estimates of these parameters using the training vectors,

$$\mu = E[\mathbf{x}], \tag{1}$$

$$\Sigma = E[(\mathbf{x}-\mu)(\mathbf{x}-\mu)^T]. \tag{2}$$

The *Mahalanobis distance* calculates the distance of a given point from the mean value for a given class normalized by the variance of the training vectors in that direction. For a given class, k, the distance is defined as,

$$d_k(\mathbf{x}) = (\mathbf{x} - \mu_\mathbf{k})^T \Sigma^{-1} (\mathbf{x} - \mu_\mathbf{k})^T. \quad (3)$$

Classification is then performed by selecting the class for which the *Mahalanobis distance* is minimized. This classification scheme was chosen because it is simple to implement and it provides reasonable results for a variety of statistical properties. More complicated classification algorithms abound and the appropriate choice for this application is an open research area. Simple neural network classifiers were also tested and found to yield similar results to those reported in Section 5.

There are several other promising classification techniques available. Supervised artificial neural networks and support vector machines both have promise in the context of classifying THz wave data.

Artificial Neural Networks (ANN) are among the most popular classification architectures in use.[21] They derive their inspiration from the operation of human and animal brains which are based on a network of very simple building blocks called neurons. In a similar manner ANNs consist of a network of simple processing elements which conventionally consist of a non-linear activation function applied to the sum of the weighted inputs. The weights of the neurons are adapted to the training data to train the neural network and then the classifier can be used to classify subsequent test vectors.

Support Vector Machines (SVMs) are another relatively recent approach to pattern recognition which has attracted a great deal of interest for a number of machine learning applications. SVM theory was first introduced by Vapnik and is based on the principle of Structural Risk Minimization.[22] Intuitively, given the set of samples belonging to two classes, SVMs learn the boundary between these two classes by mapping the input samples to a high dimensional space and then finding a hyperplane in this high dimensional space that separates the samples of the two classes. Computing the best hyperplane is posed as a constrained optimization problem and solved using quadratic programming techniques.

4.1. Feature Extraction

THz-TDS is typically used to characterize thin films or planar semi-conductor targets. In such cases the THz wave propagation can be easily modelled and the complex refractive index of the material may be extracted. For more general targets featuring scattering and diffraction the time domain pulse may be significantly distorted. Previous authors have applied linear filter models to extract features from THz pulses[15, 16] and linear transforms such as the wavelet and Karhunen Loeve transform. In this paper we attempt to perform the classification in the frequency domain. However, for the powders considered, a visual analysis did not reveal any significant absorption resonances to base the classification algorithm (see Section 5). Our system provides a frequency resolution of 37.5 GHz and a useful bandwidth of approximately 2.5 THz therefore there are up to 70 usable frequency coefficients. In practice these coefficients will contain much redundant and even misleading information and a classifier based on all 60 frequency components will prove computationally inefficient and will have poor generalization performance.

We deconvolve the measured THz responses by dividing the frequency domain responses by the reference THz spectrum which is measured without a sample in place. Due to the coherent properties of THz-TDS this yields the amplitude and phase of the sample response at each frequency so both of these components are used as potential classification features. Several methods have been proposed to reduce the number of input features. Genetic algorithms and principle component analysis are commonly used examples.[23] In this case we used random iteration to identify feature frequencies.

5. RESULTS

The THz response of a powder may generally be characterized according to the frequency dependent refractive index, absorption coefficient and scattering properties of the powder. These will depend both on the specific material and on the particle size of the powder.[24] Figure 4 shows the time domain responses for several of the powders after transmission through 2 mm of each powder. The weakest signals are seen for the powders with larger particle size (eg: sugar, salt etc). For these powders the particle size is close to the wavelength of the THz

radiation and results in strong scattering of the incident radiation. This is also evident in the frequency domain shown in fig. 5

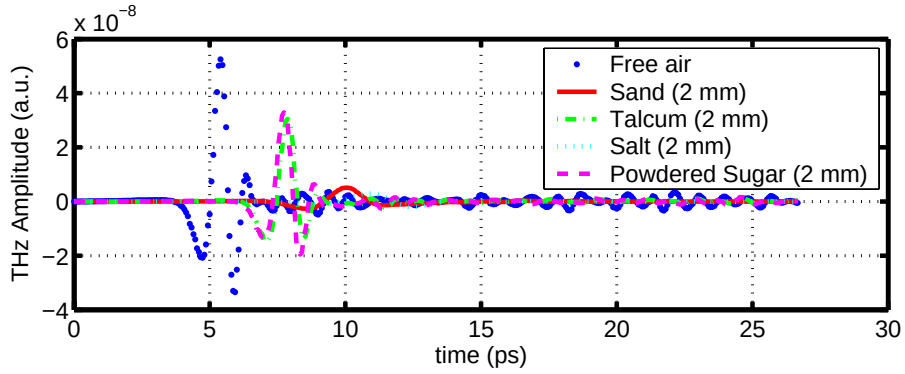

Fig. 4. THz pulses after transmission through 2 mm of various powders.

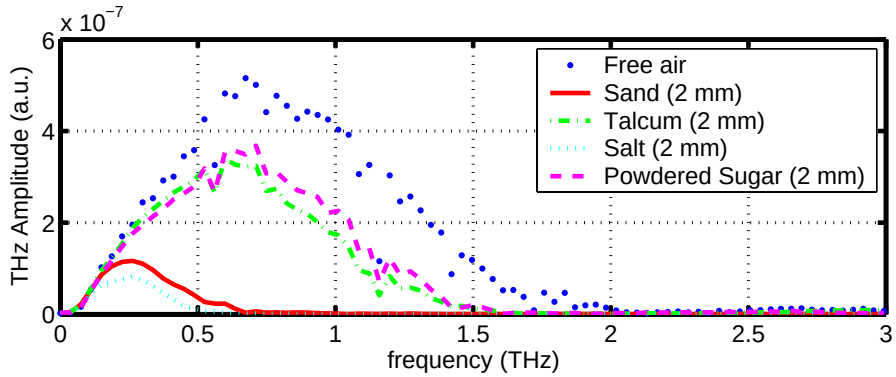

Fig. 5. THz spectra after transmission through 2 mm of various powders. The absorption peaks at 0.56 and 1.16 THz are due to water vapor absorption

As the thickness of the powders were varied the THz pulse showed a linear increase in phase (or delay of the time domain pulse) and an exponential decay in amplitude with thickness. This is illustrated in figs 6 and 7 for flour of thicknesses 1,2,3 and 4 mm.

5.1. Classification

We used the data at the extreme thicknesses (1 mm and 4 mm) to train the classifier and then tested the accuracy of the classifier using the data for thicknesses of 2 and 3 mm. This tested the ability of the classifier to accurately detect powders at different thicknesses to those at which it was trained. This is obviously an important consideration in real world detection problems.

The first question to answer was the required number of features (frequencies) needed to ensure adequate classification performance. For a given number of features, N, we used a computer to randomly select N different frequencies (within the bandwidth of 2.5 THz). We then used the deconvolved amplitude and phase of the training data at those frequencies to train the classifier and tested the resultant classification accuracy on the test data. The accuracy was recorded and a new set of random frequencies was chosen. This process was repeated 10,000 times and the highest accuracy and the corresponding frequencies were noted. This procedure was repeated for $N = 1$ .. 20, and the resultant maximum accuracy is shown in fig 8. For very low N there is insufficient

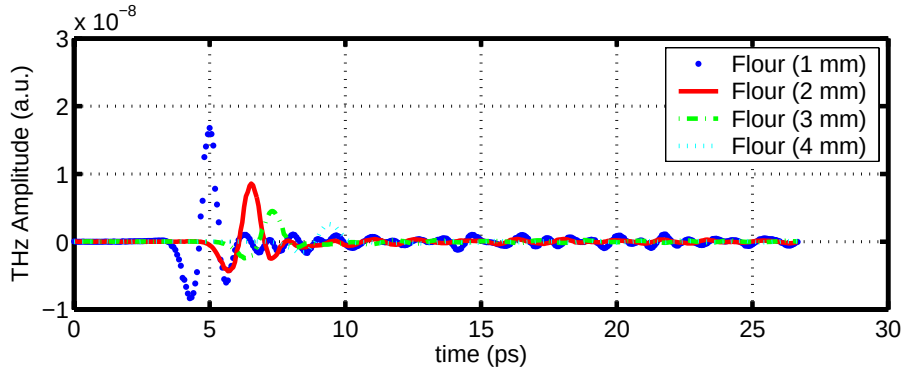

Fig. 6. THz pulses after transmission through varying thickness of flour.

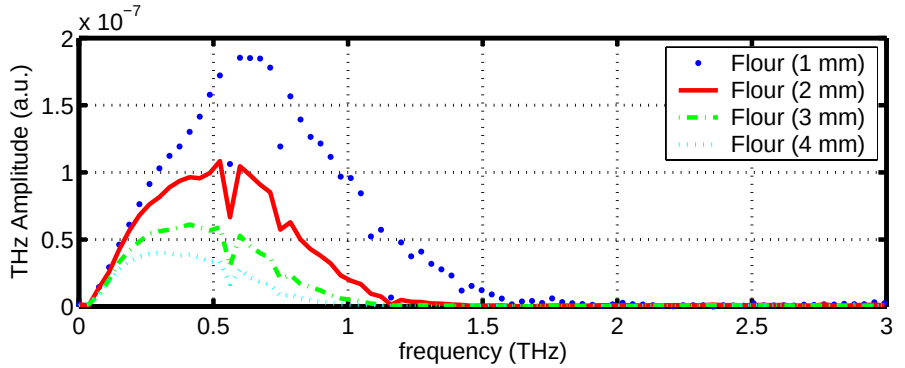

Fig. 7. THz spectra after transmission through varying thickness of flour.

information to allow a successful classification, however at $N = 8$, the classification accuracy plateaus at a near perfect level. We use this number of frequencies for the subsequent tests as it provides optimal classification accuracy and generalization ability. The frequencies resulting in the maximal classification accuracy were: 0.45, 0.90, 1.08, 1.45, 1.87, 2.06, 2.20, 2.43 THz.

The *confusion matrices* for this classifier is given below where the element, $[i, j]$, shows the relative proportion of samples belonging to class i that were recognized as class j. The classes were free air(1), sand(2), talcum powder(3) powdered sugar(4), sugar(5), baking soda(6) and flour(7).

$$\begin{bmatrix} 1.0000 & 0 & 0 & 0 & 0 & 0 & 0 \\ 0 & 0.9216 & 0 & 0 & 0.0392 & 0 & 0.0392 \\ 0 & 0 & 1.0000 & 0 & 0 & 0 & 0 \\ 0 & 0 & 0 & 1.0000 & 0 & 0 & 0 \\ 0 & 0.0098 & 0 & 0 & 0.9608 & 0 & 0.0294 \\ 0 & 0 & 0 & 0 & 0 & 1.0000 & 0 \\ 0 & 0 & 0 & 0 & 0 & 0 & 1.0000 \end{bmatrix}. \quad (4)$$

This classifier was then tested on the envelope image described in Section 3. This posed a more difficult classification problem because the paper, envelope and tape each provide additional distortions of the THz pulse. This therefore tests the ability of the classifier to generalize to real world situations.

The classifier was trained using the 8 frequency components given above. All 4 powder thicknesses were used as training data. The envelope data was then deconvolved using a reference pulse measured without the

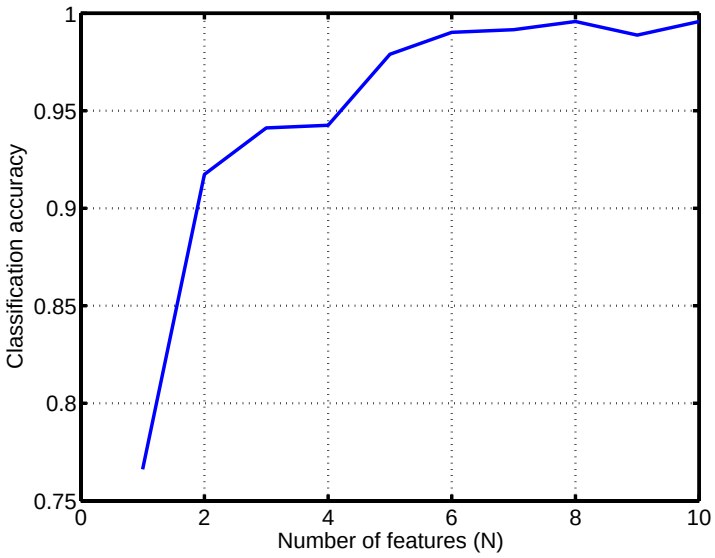

Fig. 8. Plot of maximum classifier accuracy (measured over 10,000 random ensembles of frequency components) vs the number of frequencies.

envelope in the THz beam path. A THz amplitude image is shown in fig. 9. This image was generated by plotting the amplitude of the THz pulse in the time domain at each pixel. The letters are visible due to the increased absorption and scattering caused by the powders. The classification result is shown in fig. 10. A pseudo color image is used to illustrate the classes assigned by the classifier to each pixel. The classes from darkest to lightest correspond to: free air, sugar, salt, flour, powdered sugar, baking soda, and talcum powder.

Comparison of this image with fig. 3 reveals that over half of the pixels of each powder are accurately classified.

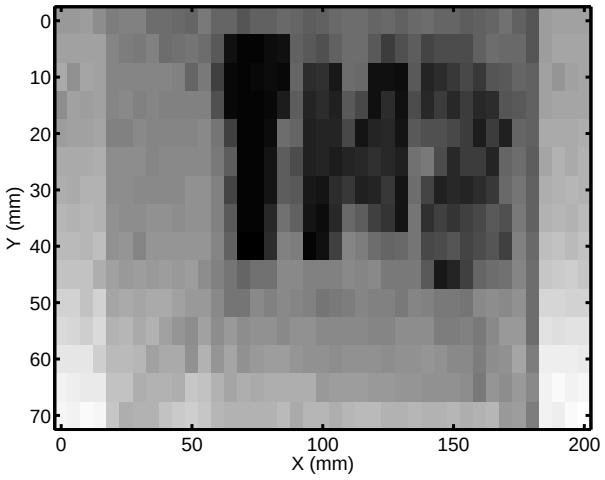

Fig. 9. THz image of an envelope containing powders taped to form the characters 'THZ'. The image was produced using the amplitude of the THz pulses in the time domain.

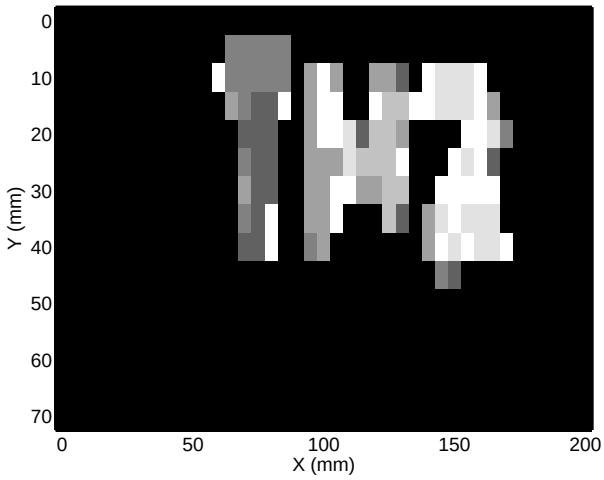

Fig. 10. THz image of an envelope containing powders taped to form the characters 'THZ'. The image was produced by classifying each pixel using a classifier trained with data for the 7 different powders at thicknesses of 1,2,3 and 4 mm. The pixel is color coded according to the class assigned by the classifier.

6. CONCLUSION

Simple feature extraction and classification algorithms were presented that allow for the automated analysis of these images and may one day facilitate automated retection of hazardous or illicit substances in mail and luggage using pulse THz imaging. Powder samples were classified using a Mahalanobis distance classifier. The required computational complexity of the classifier was reduced by iteratively refining a subset of frequency components to use as features from the measured responses.

ACKNOWLEDGMENTS

This work was supported by the Australian Research Council, the U.S. National Science Foundation, the U.S. Army Research Office and IMRA America.

This work was supported in part by the Center for Subsurface Sensing and Imaging Systems, under the Engineering Research Centers Program of the National Science Foundation (award number EEC-9986821).

REFERENCES

1. B. Ferguson and X.-C. Zhang, "Materials for terahertz science and technology," *Nature Materials* **1**(1), pp. 26–33, 2002.
2. D. Grischkowsky, S. Keiding, M. van Exter, and C. Fattinger, "Far-infrared time-domain spectroscopy with terahertz beams of dielectrics and semiconductors," *Journal of the Optical Society of America B: Optical Physics* **7**(10), pp. 2006–2015, 1990.
3. R. H. Jacobsen, D. M. Mittleman, and M. C. Nuss, "Chemical recognition of gases and gas mixtures with terahertz waves," *Optics Letters* **21**(24), pp. 2011–2013, 1996.
4. D. Arnone, C. Ciesla, and M. Pepper, "Terahertz imaging comes into view," *Physics World* (4), pp. 35–40, 2000.
5. D. M. Mittleman, M. Gupta, R. Neelamani, R. G. Baraniuk, J. V. Rudd, and M. Koch, "Recent advances in terahertz imaging," *Applied Physics B: Lasers and Optics* **68**(6), pp. 1085–1094, 1999.
6. S. Hadjiloucas, L. S. Haratzas, and J. W. Bowen, "Measurements of leaf water content using terahertz radiation," *IEEE Transactions on Microwave Theory and Techniques* **47**(2), pp. 142–149, 1999.
7. M. Knott, "See-through teeth," *New Scientist* **162**(2192), p. 22, 1999.

8. R. M. Woodward, B. Cole, V. P. Walace, D. D. Arnone, R. Pye, E. H. Linfield, M. Pepper, and A. G. Davies, "Terahertz pulse imaging of in-vitro basal cell carcinoma samples," in *Conference on Lasers and Electro-Optics 2001*, pp. 329–330, SPIE, 2001.
9. K. Douglass, "Optics firm hits obstacle in bringing sensor device to market," *Optics and Photonics News* **14**(1), pp. 22–25, 2003.
10. E. R. Brown, D. L. Woolard, A. C. Samuels, T. Globus, and B. Gelmont, "Remote detection of bioparticles in the THz region," in *IEEE MTT-S International Microwave Symposium Digest*, **3**, pp. 1591–1594, IEEE, 2002.
11. B. Ferguson and D. Abbott, "Signal processing for T-ray bio-sensor systems," in *Smart Electronics and MEMS II*, *Proceedings of SPIE* **4236**, pp. 157–169, Melbourne, Australia, 2000.
12. B. Ferguson and D. Abbott, "Wavelet de-noising of optical terahertz pulse imaging data," *Journal of Fluctuation and Noise Letters* **1**(2), pp. L65–L69, 2001.
13. L. Duvillaret, F. Garet, and J.-L. Coutaz, "Highly precise determination of optical constants and sample thickness in terahertz time-domain spectroscopy," *Applied Optics* **38**(2), pp. 409–415, 1999.
14. T. D. Dorney, R. G. Baraniuk, and D. M. Mittleman, "Material parameter estimation with terahertz time-domain spectroscopy," *Journal of the Optical Society of America A: (Optics & Vision)* **18**(7), pp. 1562–1571, 2001.
15. D. M. Mittleman, R. H. Jacobsen, R. Neelamani, R. G. Baraniuk, and M. C. Nuss, "Gas sensing using terahertz time-domain spectroscopy," *Applied Physics B: Lasers and Optics* **67**(3), pp. 379–390, 1998.
16. B. Ferguson, S. Wang, D. Gray, D. Abbott, and X.-C. Zhang, "Identification of biological tissue using chirped probe thz imaging," *Microelectronics Journal* , 2002.
17. B. B. Hu and M. C. Nuss, "Imaging with terahertz waves," *Optics Letters* **20**(16), pp. 1716–1718, 1995.
18. D. M. Mittleman, R. H. Jacobson, and M. C. Nuss, "T-ray imaging," *IEEE Journal of Selected Topics in Quantum Electronics* **2**(3), pp. 679–692, 1996.
19. Q. Wu, T. D. Hewitt, and X.-C. Zhang, "Two-dimensional electro-optic imaging of terahertz beams," *Applied Physics Letters* **69**(8), pp. 1026–1028, 1996.
20. J. Schürmann, *Pattern Classification - A Unified View of Statistical and Neural Approaches*, John Wiley & Sons, Inc., New York, 1996.
21. S. Haykin, *Neural Networks - A Comprehensive Foundation*, Macmillan College Publishing, Englandwood Cliffs, NJ, 1994.
22. V. Vapnik, *The Nature of Statistical Learning Theory*, Springer-Verlag, New York, 1995.
23. P. Biolot, E. L. Hines, M. A. Gongora, and R. S. Folland, "Electronic noses inter-comparison, data fusion and sensor selection in discrimination of standard fruit solutions," *Sensors and Actuators B (Chemical)* **88**, pp. 80–88, 2003.
24. J. Pearce and D. M. Mittleman, "Propagation of single-cycle terahertz pulses in random media," *Optics Letters* **26**(24), pp. 2002–2004, 2001.